Controlling the hybridization gap and transport in a thin-film topological insulator: Effect of strain, and electric and magnetic field

Mohammad Shafiei,[1,2] Farhad Fazileh,[1,*] François M. Peeters,[2] and Milorad V. Milošević[2,3,†]

[1]*Department of Physics, Isfahan University of Technology, Isfahan 84156-83111, Iran*
[2]*Department of Physics, University of Antwerp, Groenenborgerlaan 171, B-2020 Antwerp, Belgium*
[3]*NANOlab Center of Excellence, University of Antwerp, Antwerp, Belgium*

In a thin-film topological insulator (TI), the edge states on two surfaces may couple by quantum tunneling, opening a gap known as the hybridization gap. Controlling the hybridization gap and transport has a variety of potential uses in photodetection and energy-harvesting applications. In this paper, we report the effect of strain, and electric and magnetic field, on the hybridization gap and transport in a thin Bi_2Se_3 film, investigated within the tight-binding theoretical framework. We demonstrate that vertical compression decreases the hybridization gap, as does tensile in-plane strain. Applying an electric field breaks the inversion symmetry and leads to a Rashba-like spin splitting proportional to the electric field, hence closing and reopening the gap. The influence of a magnetic field on thin-film TI is also discussed, starting from the role of an out-of-plane magnetic field on quantum Hall states. We further demonstrate that the hybridization gap can be controlled by an in-plane magnetic field, and that by applying a sufficiently strong field a quantum phase transition from an insulator to a semimetal can be achieved.

I. INTRODUCTION

Topological insulators (TIs) typically exhibit bulk gaps in the 20–300 meV range, while maintaining the conduction edge or surface states protected by time-reversal symmetry (TRS) [1,2]. In recent years, TIs have been extensively studied both theoretically and experimentally due to their broad potential for applications. Three-dimensional TIs are typically classified as either strong or weak, in terms of the number of Dirac cones on their surfaces [1]. The Bi_2Se_3 family of materials, also known as trichalcogenide TIs, possess surface states protected by time-reversal symmetry. The electrons of these states resemble massless helical Dirac fermions in which the spin of electrons is locked to momentum [3]. Bi_2Se_3 is a strong TI that has been widely studied as a paradigmatic TI, exhibiting a single Dirac cone on its surfaces at the Γ point, robust against TRS disorders [4,5], as confirmed by angle-resolved photoemission experiments. The energy states of TI surfaces were also confirmed by scanning tunneling spectroscopy [6,7]. Bi_2Se_3 has a crystal structure with a symmetry group of $R\bar{3}m$ [8], with a unit cell consisting of five atoms: two Bi atoms and three Se atoms in layers arranged in ABCABC vertical stacking [5]. The bulk gap of Bi_2Se_3 is 290 meV, which is much larger than the energy scale at room temperature.

In the thin-film regime, controlling the hybridization gap can be a tool to optimize and control optical properties for photodetectors and energy-harvesting applications [9]. Strain

can change the topological nature of the system for values above the critical value [10]. By applying an electric field, the coupling of surface states on the top and bottom surfaces can be eliminated, leading to the quantum spin Hall effect. Out-of-plane and in-plane magnetic fields can create fascinating properties. In thin films with a hybridization gap, out-of-plane magnetic fields can form quantum anomalous Hall (QAH) states, whereas an in-plane magnetic field changes the hybridization gap, causing a quantum phase transition [11–14].

In this paper, we assess the effect of strain, and electric and magnetic field on Bi_2Se_3 thin films. Using these external means, by controlling the system gap and Dirac states in thin-film TI, one expects novel effects such as a pseudomagnetic field, helical flat bands, amd also topological phase transitions, and the appearance of the quantum Hall effect (QHE) [15]. Since the Bi_2Se_3 layers are coupled by weak van der Waals interactions, it is feasible to fabricate this material in a thin-film form [16,17]. Therefore, the study and control of its physical properties under different conditions is timely, and critical regarding possible applications of thin-film TIs in the new generation of electronic devices.

The paper is organized as follows. In Sec. II, we employ the symmetries to construct a real-space Hamiltonian based on the parameters of the four-band Hamiltonian. Next, we show how to introduce strain, and electric and magnetic fields based on the symmetries of the system. In Sec. III, the effects of biaxial and uniaxial strain are considered. We show how by applying a compressive uniaxial strain or tensile biaxial strain the hybridization-induced gap can be reduced and eventually closed. In Sec. IV, we examine the effect of electric field on the hybridization gap, followed by a discussion of the effect of applied magnetic field on three-dimensional TI and QAH

*fazileh@cc.iut.ac.ir
†milorad.milosevic@uantwerpen.be

TABLE I. Hopping parameters for the four-band Hamiltonian, obtained by fitting to the DFT data [20].

A_1' (eV Å)	A_2' (eV Å)	C_0' (eV Å)	C_1' (eV Å^2)
5.35	4.44	-0.0063	6.65
C_2' (eV Å^2)	M_0' (eV Å)	M_1' (eV Å^2)	M_2' (eV Å^2)
-1.75	0.29	-10.25	-56.6

states down to the thin-film regime in Sec. V. The latter is done by assessing the longitudinal and Hall conductance of the system using the Landauer-Büttiker formalism for different thickness of the TI. In Sec. V B we detail the effect of an in-plane magnetic field on the hybridization gap. Finally, Sec. VI summarizes our results and we present our conclusions.

II. CRYSTAL STRUCTURE AND HAMILTONIAN

Numerous studies to date have addressed the topological insulator properties of Bi$_2$Se$_3$, many of which use a four-band Hamiltonian. Using density functional theory (DFT) data and considering the states near the Fermi level, there will be four states $|P_z^\pm, \uparrow (\downarrow)\rangle$ for different parities and spins [2], so the Hamiltonian of the four bands in this basis can be expressed as follows [5,18,19],

$$H = \varepsilon_k' + \begin{pmatrix} M_k' & A_1'k_z & 0 & A_2'k_- \\ A_1'k_z & -M_k' & A_2'k_- & 0 \\ 0 & A_2'k_+ & M_k' & -A_1'k_z \\ A_2'k_+ & 0 & -A_1'k_z & -M_k' \end{pmatrix}, \quad (1)$$

where $\varepsilon_k' = C_0' + C_1'k_z^2 + C_2'k_\perp^2$, $M_k' = M_0' + M_1'k_z^2 + M_2'k_\perp^2$, and $k_\perp^2 = k_x^2 + k_y^2$. The values of the parameters used are shown in Table I.

An effective real-space Hamiltonian was employed, in which hopping parameters were determined by comparing the results of the four-band Hamiltonian to the DFT results near the Γ point. According to Fig. 1, a unit cell was considered as a set of four states that are connected by $\vec{n}_i$ vectors ($i = 1, 2, 3$). Considering the nearest neighbors, there are six neighbors for each unit cell in the x-y plane. Hopping between
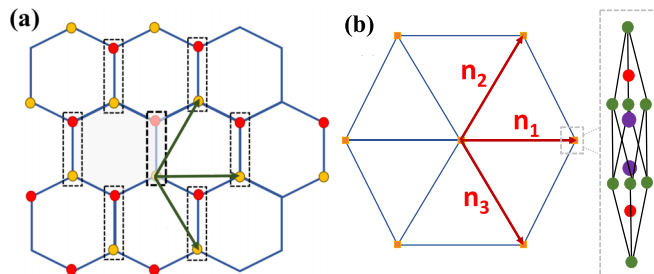

FIG. 1. (a) The lattice structure of Bi$_2$Se$_3$ in the x-y plane. (b) Each unit cell has six neighboring unit cells in the x-y plane, connected by vectors $\pm\vec{n}_i$ ($i = 1, 2, 3$). Here, $\mathbf{n}_1 = (\frac{1}{2}a, \frac{\sqrt{3}}{2}a, 0)$, $\mathbf{n}_2 = (\frac{-1}{2}a, \frac{\sqrt{3}}{2}a, 0)$, $\mathbf{n}_3 = (a, 0, 0)$.
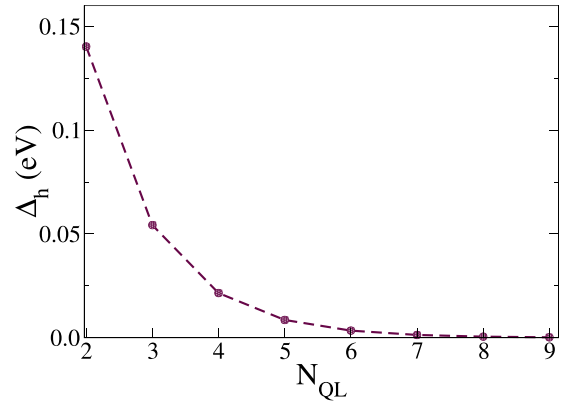

FIG. 2. Hybridization gap due to coupling of surface states, as a function of the thickness of the Bi$_2$Se$_3$ film (thickness is expressed as the number of quintuple layers N_{QL}).

these neighbors is denoted by T_α and $T_\alpha^\dagger$ ($\alpha = 1, 2, 3$). In the z direction there are two neighbors, with hoppings T_4 and $T_4^\dagger$ [21,22]. The real-space Hamiltonian is then defined as [21]

$$H = \Sigma_i c_i^\dagger E c_i + \Sigma_{i,\alpha}(c_i^\dagger T_\alpha c_{i+\alpha} + \text{H.c.}), \quad (2)$$

where $\alpha = 1, 2, 3, 4$, the operator $c_i^\dagger$ (c_i) creates (annihilates) an electron at site i, and E and T_α are on-site energy and hopping parameters between unit cells, respectively, defined as

$$E = (E_0 - 2\Sigma_\alpha B_\alpha)\sigma_z \otimes \sigma_0, \quad (3)$$

$$T_\alpha = C_\alpha \sigma_0 \otimes \sigma_0 + B_\alpha \sigma_z \otimes \sigma_0 - i\left(\frac{A_\alpha}{2}\right)\sigma_x \otimes \vec{\sigma} \cdot \vec{n}_\alpha. \quad (4)$$

Regarding the symmetries of the system, A_{n_1,n_2,n_3}, B_{n_1,n_2,n_3}, C_{n_1,n_2,n_3}, that are related to the x-y plane parameters, are isotropic. Thus we adopt the following notation for the in-plane parameters $A_{n_1,n_2,n_3} = A_2$, $B_{n_1,n_2,n_3} = B_2$, $C_{n_1,n_2,n_3} = C_2$, and for out-of-plane parameters we use $A_{n_4} = A_1$, $B_{n_4} = B_1$, and $C_{n_4} = C_1$. Further, for the values of the hopping parameters we take $(A_1, A_2, B_1, B_2, C_1, C_2) = (A_1', A_2', M_1', M_2', C_1', C_2')$.

When the thickness of the TI is reduced to several nanometers (i.e., the thin-film regime), the surface states on the top and bottom surfaces overlap and couple, leading to hybridization and opening of a gap (usually referred to as hybridization gap) [16,23]. Figure 2 shows the gap as a function of the film thickness (in units of quintuple layers N_{QL}). For thickness above 8 QLs, the hybridization gap vanishes (the overlap of surface states is negligible) [24,25].

Next, we will indicate how to introduce effects of strain, and electric and magnetic field in our model. Strain is defined as changes in the displacement vector $\vec{U}$ relative to the pristine position, and can be expressed by the following tensor [9]:

$$\varepsilon_{ij} = \frac{1}{2}\left(\frac{\partial U_i}{\partial x_j} + \frac{\partial U_j}{\partial x_i}\right). \quad (5)$$

The strain tensor ε_{ij} includes six independent components, three of which are for uniaxial strain ($\varepsilon_{xx}, \varepsilon_{yy}, \varepsilon_{zz}$) and the other three for shear strain ($\varepsilon_{xy} = \varepsilon_{yx}, \varepsilon_{xz} = \varepsilon_{zx}, \varepsilon_{yz} = \varepsilon_{zy}$). In the next section, the influence of strain on the hopping

parameters and the topological behavior of thin-film Bi_2Se_3 will be assessed. The strain changes the bond length and bond angles, thereby altering the Hamiltonian parameters. According to the system symmetries, the following terms are added to the system hopping:

$$E_0 \rightarrow (E_0 + \tilde{E}_1 \epsilon_{zz} + \tilde{E}_2 \epsilon_+)\sigma_z \otimes \tau_0, \quad (6)$$

$$T_\alpha \rightarrow \tilde{A}_\alpha \epsilon_\alpha \sigma_x \otimes \vec{\sigma} \cdot \vec{n}_\alpha. \quad (7)$$

We take the values of these parameters from Ref. [26]. The application of a perpendicular electric field also adds a term to the on-site energy hopping according to the symmetries of the system [9],

$$H_E = \left(I_{QL} - \frac{N_{QL}}{2} \right) c\, E_z\, \sigma_y \otimes \sigma_z = V\, \sigma_y \otimes \sigma_z, \quad (8)$$

where $I_{QL} \in [1, N_{QL}]$, c is the lattice parameter in the z direction and E_z is the z component of the electric field. Finally, when applying the magnetic field to the system, both Zeeman and orbital effects must be considered. For the applied field B_z, the orbital effect is introduced through the Peierls substitution. Concerning the Zeeman effect, the following term is added to the on-site energy Hamiltonian, using the system symmetries [18,27],

$$H_{Zeeman} = M_i\, \sigma_0 \otimes \sigma_i, \quad (9)$$

for $i = x, y, z$ and with a Zeeman exchange field $M_i = \frac{\mu_B}{2}(g_i B_i)$, where $\mu_B = \frac{e\hbar}{2m_0}$.

III. EFFECT OF STRAIN

It is a well known that straining thin films can yield more pronounced effects compared to straining bulk crystals. Furthermore, when a TI thin film is placed on a substrate, a lattice mismatch is imposed on the TI at the contact surface, potentially causing strain [10]. Using an atomic force microscope probe, strain can also be induced by external force loading [10].

Therefore, in this section, the effect of strain on a few layers of Bi_2Se_3 is explored. We start from the effect of the out-of-plane uniaxial strain, applied by extending or compressing the lattice parameter in the z direction (c) as $\epsilon_\perp = \frac{c-c_0}{c_0}$, where c_0 is the lattice parameter in the z direction in the strain-free structure [4]. By applying a compressive uniaxial strain in the z direction to the system, the gap of the system was first increased; eventually, an indirect gap was formed and then the gap was closed and the system entered the metallic phase. The tensile uniaxial strain reduced the gap and eventually closed the bulk gap. Strain also affected the wave function of the surface states and the hybridization gap resulting from these states and the penetration depth of these wave functions. It should be noted that the surface states' band gap behaves opposite to the bulk band gap [9,28].

As shown in Fig. 3, compressive out-of-plane strain reduces the gap, because of increasing the Coulomb interaction between sites and the hopping parameter between them. The hybridization-induced gap was decreased and subsequently closed by applying $\epsilon_\perp = -6\%$ compressive strain for $N_{QL} > 3$. However, it should be noted that observing the topological phase transition with a strain of -6% is experimentally
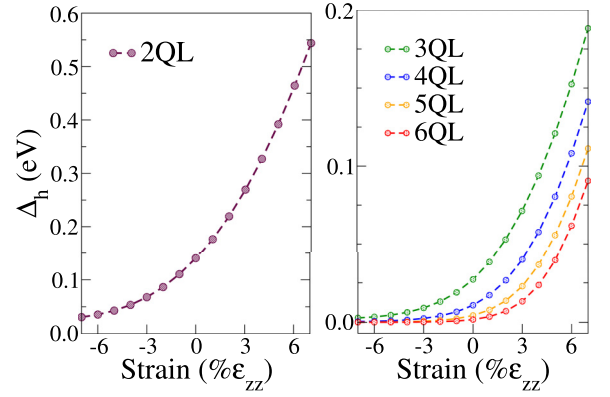

FIG. 3. Hybridization gap under uniaxial strain. Compressive strain reduces the distance by increasing the Coulomb interaction and hopping parameter between the sites. The hybridization-induced gap is decreased and eventually closed around 6% of strain when compressive strain is applied.

challenging and requires 2 GPa uniaxial stress. Chemical substitution can be used to apply strain on this scale in some situations [26].

The van der Waals type of bonding between QLs is weaker than covalent interactions between atomic layers inside a QL, therefore out-of-plane strain is not homogeneous along the z axis. Liu *et al.* [8], for example, demonstrated that applying strain in the z direction increased the thickness of a QL much less than the distance between the QLs. It is also demonstrated in the same work that the topological phase transition is mostly influenced by the interlayer interaction.

The in-plane biaxial strain is defined as $\epsilon_{bia} = \frac{a-a_0}{a_0}$, by extending or compressing the lattice parameter in the x-y plane, where a_0 is the lattice parameter in the x-y plane for the unstrained structure. For compressive biaxial strain ($\epsilon_\parallel < 0$), the parameter c tends to increase while for tensile biaxial strain ($\epsilon_\parallel > 0$) the parameter c exhibits a decreasing trend. The hybridization gap found in a Bi_2Se_3 thin film as a function of biaxial in-plane strain is depicted in Fig. 4. The gap induced by hybridization was increased by compressive biaxial strain, while being decreased by tensile biaxial strain. At a strain
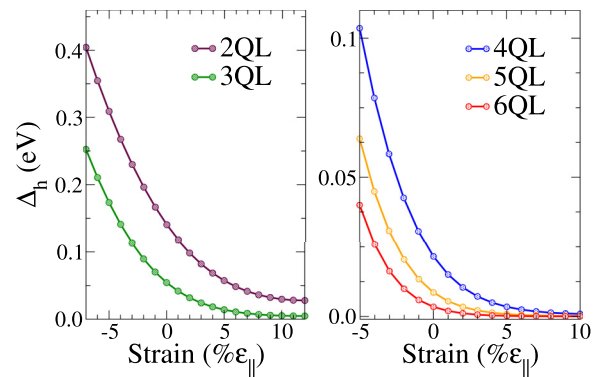

FIG. 4. Hybridization gap under biaxial strain. The gap generated by hybridization is enlarged by compressive biaxial strain, whereas tensile biaxial strain shrinks the gap, and the gap is finally closed at a strain level of 8% for $N_{QL} > 3$.
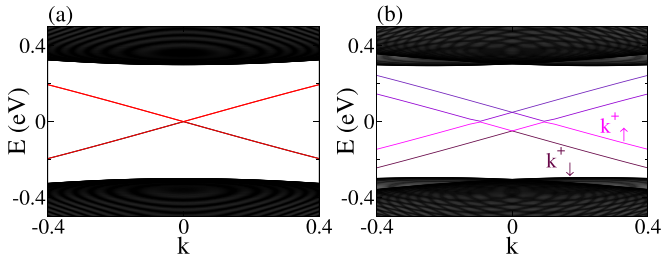
FIG. 5. The effect of an external electric field on the surface states. The surface bands' degeneracy is removed by applying an electric field perpendicularly to the surface.

FIG. 6. The density $|\Psi_\uparrow(k+\uparrow, z)|^2$ (red line), and $|\Psi_\downarrow(k+\downarrow, z)|^2$ (blue line) for a Bi_2Se_3 film (a) without and (b) with an applied electric field.

level of 8%, the gap was finally closed for $N_{QL} > 3$. Biaxial strain changed the lattice parameter c in the z direction, closing the band gap at Γ. As a result, applying a biaxial strain has an indirect effect on the band gap. The Poisson ratio ν describes the dependence of uniaxial out-of-plane strain on biaxial in-plane strain as follows [29]:

$$\frac{\epsilon_\perp}{\epsilon_\parallel} = -\frac{2\nu}{1-\nu}. \qquad (10)$$

Bi_2Se_3 has a Poisson ratio of 0.27, which is consistent with previous calculations [4,30].

IV. EFFECT OF AN EXTERNAL ELECTRIC FIELD

Due to the increase of coupling of surface states on the top and bottom surfaces with decreasing TI thickness, the topological phase of the material can change from a two-dimensional TI to a trivial insulator [23,31]. Applying an electric field is one possible approach to manage this connection, as the coupling of surface states can be removed and the quantum spin Hall effect can be observed in the presence of an appropriate electric field [31]. The contribution of the electric field is added to the Hamiltonian through the following term,

$$e\frac{\epsilon_0}{\epsilon_0 + \epsilon_r}F_z z = eE_z z, \qquad (11)$$

where $\epsilon_0 = 1$ and $\epsilon_r = 113$ are dielectric constants for air and Bi_2Se_3, respectively. However, it should be emphasized that a strong electric field can change the properties of the surface state. Surface states are spin degenerate in the absence of electric field. The surface bands' degeneracy can be removed by applying an electric field perpendicular to the surface for a particular energy. As a result, the wave functions for up- and down-spin states are not the same [31] (see Figs. 5 and 6). The inversion symmetry is broken by applying an electric field, which causes a Rashba-like spin splitting corresponding to the electric field.

As shown in Fig. 7, increasing the electric field perpendicular to the film plane causes the hybridization gap to close, and then reopen and increase. The topological characteristics of the thin film can thereby be controlled by applying an appropriate electric field, and a topological phase transition between topologically trivial and nontrivial states has been observed [32].
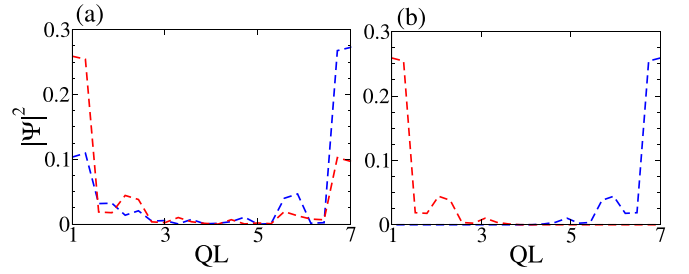
V. EFFECT OF MAGNETIC FIELD

A. Out-of-plane field

In this section, we examine the effect of an out-of-plane magnetic field on a three-dimensional TI in the thin-film regime. A Zeeman field or exchange field (M_z) arises when a three-dimensional (3D) TI is exposed to a perpendicular magnetic field (in the z direction in our case), and the electrons on each surface obtain different properties. The Dirac cone is shifted on the lateral surfaces because of an effectively in-plane magnetic field there, whereas the Dirac cone is gapped on the top and bottom surfaces by an energy gap Δ (equal to $2M_z$) [21,33] as shown in Fig. 8. The Zeeman or exchange field, as well as the hybridization gap, have different effects on the properties of the mass of Dirac fermions and can be utilized to modify the surface state. The presence of exchange energy in 3D TI thin films changes the model to a Haldane one, in which the exchange energy acts as staggered fluxes and the hybridization gap acts as an alternating on-site energy [14]. The longitudinal and Hall conductance of the 3D TI Bi_2Se_3 system was evaluated using the Landauer-Büttiker formalism for different numbers of layers (N_{QL}) in the thin-film regime under a perpendicular magnetic field. For further reference, we consider a four-lead setup, with leads 1 and 3 along the x direction and leads 2 and 4 in the y direction [34]. The conductivity between the p and q leads in a four-terminal setup can be represented in terms of a transmission coefficient (T_{pq}) in the Landauer-Büttiker formalism as
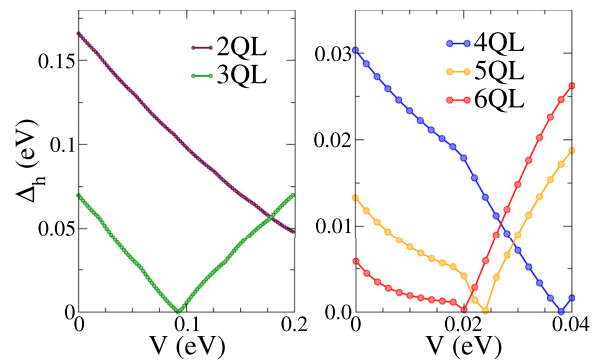

FIG. 7. Hybridization gap in the presence of an electric field for different film thicknesses (expressed as N_{QL}). The gap induced by hybridization reduces, closes, and then reopens and increases when increasing the electric field.
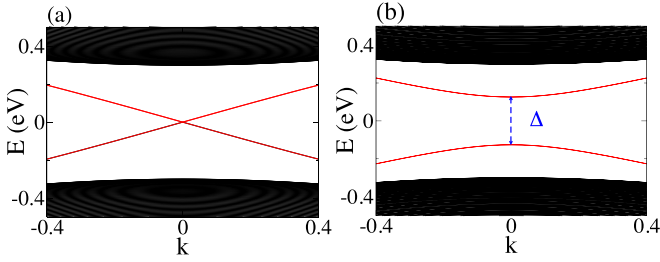
FIG. 8. Effect of an out-of-plane magnetic field on the surface states in a 3D TI. The Zeeman effect, also known as the exchange field (M_z), arises when a magnetic field is applied perpendicularly to the surfaces. The Dirac cones on the top and bottom surfaces are gapped ($\Delta = 2M_z$).

$T_{pq} = \text{Tr}[\Gamma_p G^r \Gamma_q G^a]$, where Γ_p is the self-energy in lead p, G^r is the retarded Green's function, and G^a is the advanced Green's function [21,35].

A biasing voltage is applied between leads 1 and 3 in this setup, and the current between leads 1 and 3 is measured to obtain the longitudinal conductance (σ_{xx}), whereas the current observed between leads 2 and 4 yields the Hall conductance (σ_{xy}):

$$\sigma_{xx} = T_{13}\frac{e^2}{h} = G_{xx}\frac{e^2}{h},$$

$$\sigma_{xy} = (T_{14} - T_{12})\frac{e^2}{h} = G_{xy}\frac{e^2}{h}. \quad (12)$$

The Hall transport calculations in terms of energy for the different numbers of layers are shown in Fig. 9. In the 3D TI thin film, an external magnetic field induces an integer quantum Hall (IQH) state. The topological state of quantum matter known as the integer quantum Hall effect (IQHE) has zero longitudinal conductivity and a Hall conductance that is an integer multiple of the quantum conductance. The number of
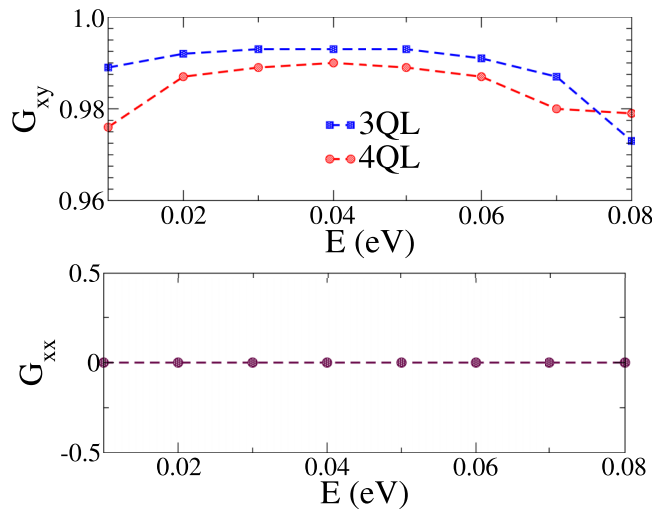

FIG. 9. Hall conductance G_{xy} as a function of energy for films of thicknesses 3 QLs and 4 QLs, determined by Landauer-Büttiker formalism. When an external magnetic field is applied to a 3D TI thin film while $G_{xx} = 0$, quantum Hall states are formed ($L = 15$, $M_z = \Delta_h$).
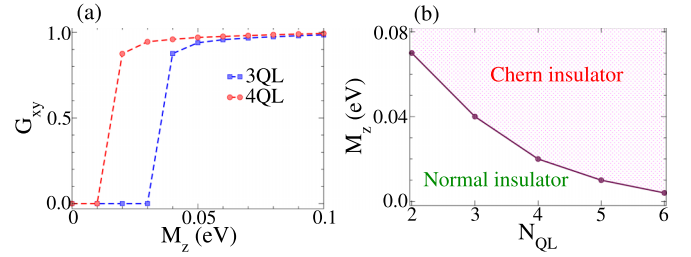

FIG. 10. (a) Hall conductance for $N_{QL} = 3$ and $N_{QL} = 4$. G_{xy} is initially zero, before QHE states emerge as the Zeeman exchange increases. (b) Phase diagrams for different N_{QL} as a function of the Zeeman exchange.

conducting chiral channels on the surface is determined by an integer C (i.e., the topology invariant of the quantum phase). This parameter is robust against impurities and electron interactions. The inverse symmetry is broken in the thin-film regime, and C will be an integer ($\sigma_{xy} = C\frac{e^2}{h}$) [33,36,37].

Applying a magnetic field results in a Haldane model realization for a 3D TI in the thin-film regime, in which the exchange field (M_z) serves as staggered fluxes and the hybridization gap (Δ_h) is equivalent to alternating on-site energy. We only have one shift in Landau levels if $M_z \neq 0$ and $\Delta_h = 0$. Landau levels will be odd ($C = 0, 1, 3, 5, \ldots$) if $M_z = 0$ and $\Delta_h \neq 0$. Finally, if $M_z \neq 0$ and $\Delta_h \neq 0$, Landau plateaus exist for all integer values of C ($C = 1, 2, 3, 4, \ldots$) [14].

For the 3-QL and 4-QL samples, Fig. 10 shows our G_{xy} results. Initially, $G_{xy} = 0$ in the presence of a small magnetic field. A topological phase transition from a normal insulator to a Chern insulator eventually occurs as the Zeeman exchange increases. Also displayed are the critical values for samples with different N_{QL}, which are different for each sample due to the different hybridization gap.

The application of a vertical magnetic field leads electrons on the lateral surfaces to experience an in-plane magnetic field, shifting the Dirac fermions on these surface states, as previously mentioned. The transmission coefficients for
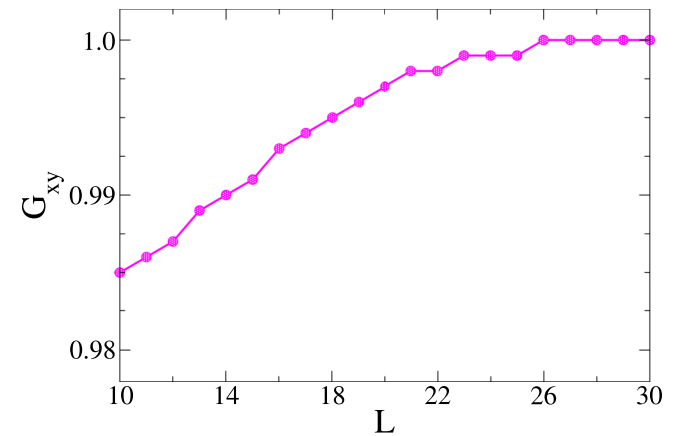

FIG. 11. Hall conductance for $N_{QL} = 3$ for different L ($= N_x = N_y$). The effect of lateral surfaces decreases as L increases, and the transmission coefficient approaches one ($M_z = \Delta_h$).

different lateral sizes L ($L = N_x = N_y$, where N_x and N_y are the number of unit cells in the x and y directions, respectively), for 3-QL and 4-QL samples are depicted in Fig. 11. As can be seen, the value of the transmission coefficients approaches one as the number of unit cells in the x and y directions is increased, resulting in quantum Hall states.

B. In-plane magnetic field

Low-energy excitations in TIs behave similarly to massless Dirac particles, which have gained a lot of attention in recent years [6,38–40]. Dirac points can be gapped or merging and annihilating by breaking symmetries that preserve them, such as TRS [41,42]. At low temperatures, the behavior of thick- and thin-film systems differs in the presence of an in-plane magnetic field. Dirac cones will have no gaps on the top and bottom surfaces and will contain opposing spin helicity when the TI is thick enough [11].

The application of the in-plane magnetic field appears as a vector potential in the Dirac Hamiltonian surface states when dealing with a 3D TI, and its effect may be eliminated by using the gauge transformation to the surface electron wave functions. A diamagnetic response emerges in the thin-film regime if the Fermi energy is inside the hybridization gap, and a quantum phase transition from an insulator to a semimetal occurs for a critical value of the in-plane magnetic field. For concreteness, assume the in-plane magnetic field is along the x-axis direction, while the z axis is perpendicular to the film plane. The effect of the in-plane magnetic field on the helical surface electrons could be removed by a gauge transformation of the electron field operator as $\Psi(\mathbf{r}) \rightarrow \Psi(\mathbf{r}) \exp(ik_B y \tau_z)$, which shifts Dirac cones by $\pm k_B$ along the y axis. The phase factor is complex conjugated at the top and bottom surfaces, which breaks the gauge symmetry [11,12].

In a semiclassical regime, considering spin-helical surface-state electrons whose spin direction is in the direction of the magnetic field B, the spin magnetic moment and the orbital magnetic moment are

$$\mu_{\text{spin}} = -g\mu_B/2,$$

$$\mu_{\text{orb}} = \frac{e}{2(w+t)/v_F} wt = et v_F/2, \tag{13}$$

where μ_B represents the Bohr magneton, g is the in-plane spin g factor, and w and t indicate the sample width and thickness, respectively (for a thin film $w \gg t$) [43]. The effective Zeeman energy is defined as follows, considering the spin and orbital magnetic moment:

$$E_B = g_{\text{eff}} \mu_B B = (g\mu_B - et v_F)B. \tag{14}$$

The hybridization gap Δ_h in the absence of an in-plane magnetic field will decrease if an in-plane magnetic field is applied. The hybridization gap will finally reach zero for a critical value of the magnetic field, as shown in Fig. 12.
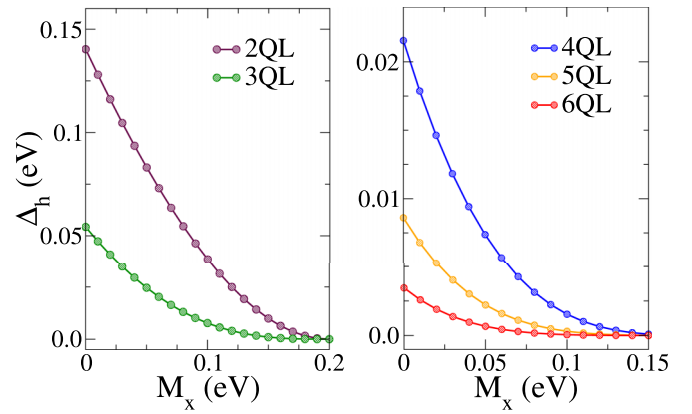

FIG. 12. The effect of an in-plane magnetic field on the hybridization gap. The hybridization gap decreases and eventually disappears when an in-plane magnetic field is applied, leading to a quantum phase transition from an insulator to a semimetal.

The Dirac points on the top and bottom surfaces are restored when the magnetic field is increased further, and one has separate 2D topological semimetal behaviors as long as the translational symmetry is maintained [11,12].

VI. CONCLUSIONS

In summary, we analyzed the behavior of thin-film topological insulators using a real-space tight-binding Hamiltonian for Bi_2Se_3. We show that strain, and electric and magnetic fields can be used to control the hybridization gap and transport in such films, which has an impact on a broad range of ongoing experiments as well as potential device applications. We showed that uniaxial strain increases the hybridization gap, while biaxial strain has the opposite effect. We further revealed that a perpendicular electric field (gating) results in a Rashba-like spin splitting proportional to the electric field, closing and reopening the gap with increasing field. The presence of a hybridization gap in the thin-film regime results in integer quantum Hall effect (IQHE) states only for Zeeman exchange values larger than the critical value ($\approx \Delta_h/2$), as we determined by detailing the effect of the applied *out-of-plane* magnetic field. Beyond this critical value, the exchange field effect takes precedence over the finite-size gap (Δ_h), and the QHE state emerges. Finally, we show that the hybridization gap decreases and eventually vanishes with increasing *in-plane* magnetic field, resulting in a quantum phase transition from an insulator to a semimetal.

[1] K.-H. Zhang, Z.-C. Wang, Q.-R. Zheng, and G. Su, Phys. Rev. B **86**, 174416 (2012).

[2] D. Hsieh, D. Qian, L. Wray, Y. Xia, Y. S. Hor, R. J. Cava, and M. Z. Hasan, Nature (London) **452**, 970 (2008).

[3] H. Aramberri and M. Muñoz, J. Phys.: Mater. **1**, 015009 (2018).

[4] H. Aramberri and M. C. Muñoz, Phys. Rev. B **95**, 205422 (2017).

[5] H. Zhang, C.-X. Liu, X.-L. Qi, X. Dai, Z. Fang, and S.-C. Zhang, Nat. Phys. **5**, 438 (2009).

[6] M. Z. Hasan and C. L. Kane, Rev. Mod. Phys. **82**, 3045 (2010).

[7] M. Tahir and U. Schwingenschlögl, Phys. Rev. B **86**, 075310 (2012).

[8] W. Liu, X. Peng, C. Tang, L. Sun, K. Zhang, and J. Zhong, Phys. Rev. B **84**, 245105 (2011).

[9] M. R. Brems, J. Paaske, A. M. Lunde, and M. Willatzen, New J. Phys. **20**, 053041 (2018).

[10] R. Battilomo, N. Scopigno, and C. Ortix, Phys. Rev. B **100**, 115131 (2019).

[11] Y. Xu, G. Jiang, I. Miotkowski, R. R. Biswas, and Y. P. Chen, Phys. Rev. Lett. **123**, 207701 (2019).

[12] A. A. Zyuzin, M. D. Hook, and A. A. Burkov, Phys. Rev. B **83**, 245428 (2011).

[13] J. Wang, B. Lian, H. Zhang, Y. Xu, and S.-C. Zhang, Phys. Rev. Lett. **111**, 136801 (2013).

[14] H. Li, L. Sheng, and D. Y. Xing, Phys. Rev. B **84**, 035310 (2011).

[15] D. Flötotto, Y. Bai, Y.-H. Chan, P. Chen, X. Wang, P. Rossi, C.-Z. Xu, C. Zhang, J. A. Hlevyack, J. D. Denlinger, H. Hong, M.-Y. Chou, E. J. Mittemeijer, J. N. Eckstein, and T.-C. Chiang, Nano Lett. **18**, 5628 (2018).

[16] C.-X. Liu, H. J. Zhang, B. Yan, X.-L. Qi, T. Frauenheim, X. Dai, Z. Fang, and S.-C. Zhang, Phys. Rev. B **81**, 041307(R) (2010).

[17] H. Peng, K. Lai, D. Kong, S. Meister, Y. Chen, X.-L. Qi, S.-C. Zhang, Z.-X. Shen, and Y. Cui, Nat. Mater. **9**, 225 (2010).

[18] C.-X. Liu, X.-L. Qi, H. J. Zhang, X. Dai, Z. Fang, and S.-C. Zhang, Phys. Rev. B **82**, 045122 (2010).

[19] S. Mao, A. Yamakage, and Y. Kuramoto, Phys. Rev. B **84**, 115413 (2011).

[20] I. Aguilera, C. Friedrich, and S. Blügel, Phys. Rev. B **100**, 155147 (2019).

[21] R.-L. Chu, J. Shi, and S.-Q. Shen, Phys. Rev. B **84**, 085312 (2011).

[22] R. Chen, S. Li, H.-P. Sun, Q. Liu, Y. Zhao, H.-Z. Lu, and X. C. Xie, Phys. Rev. B **103**, L241409 (2021).

[23] J. Linder, T. Yokoyama, and A. Sudbø, Phys. Rev. B **80**, 205401 (2009).

[24] Y. Zhang, K. He, C.-Z. Chang, C.-L. Song, L.-L. Wang, X. Chen, J.-F. Jia, Z. Fang, X. Dai, W.-Y. Shan *et al.*, Nat. Phys. **6**, 584 (2010).

[25] Y. S. Hou, J. W. Kim, and R. Q. Wu, Phys. Rev. B **101**, 121401(R) (2020).

[26] S. M. Young, S. Chowdhury, E. J. Walter, E. J. Mele, C. L. Kane, and A. M. Rappe, Phys. Rev. B **84**, 085106 (2011).

[27] T. Sabze and H. Cheraghchi, Phys. Rev. B **96**, 155440 (2017).

[28] X. Luo, M. B. Sullivan, and S. Y. Quek, Phys. Rev. B **86**, 184111 (2012).

[29] M. Ohring, *Materials Science of Thin Films* (Elsevier, Amsterdam, 2001).

[30] X. Gao, M. Zhou, Y. Cheng, and G. Ji, Philos. Mag. **96**, 208 (2016).

[31] G. Liu, B. Zhou, and G. Zhou, Phys. Lett. A **380**, 3650 (2016).

[32] G. Liu, G. Zhou, and Y.-H. Chen, Appl. Phys. Lett. **101**, 223109 (2012).

[33] S.-B. Zhang, H.-Z. Lu, and S.-Q. Shen, Sci. Rep. **5**, 13277 (2015).

[34] J. Li, L. Hu, and S.-Q. Shen, Phys. Rev. B **71**, 241305(R) (2005).

[35] S. Datta, *Electronic Transport in Mesoscopic Systems* (Cambridge University Press, Cambridge, UK, 1997).

[36] W.-Y. Shan, H.-Z. Lu, and S.-Q. Shen, New J. Phys. **12**, 043048 (2010).

[37] H.-Z. Lu, W.-Y. Shan, W. Yao, Q. Niu, and S.-Q. Shen, Phys. Rev. B **81**, 115407 (2010).

[38] A. H. Castro Neto, F. Guinea, N. M. R. Peres, K. S. Novoselov, and A. K. Geim, Rev. Mod. Phys. **81**, 109 (2009).

[39] N. P. Armitage, E. J. Mele, and A. Vishwanath, Rev. Mod. Phys. **90**, 015001 (2018).

[40] L. Tarruell, D. Greif, T. Uehlinger, G. Jotzu, and T. Esslinger, Nature (London) **483**, 302 (2012).

[41] M. Bellec, U. Kuhl, G. Montambaux, and F. Mortessagne, Phys. Rev. Lett. **110**, 033902 (2013).

[42] Y. Hasegawa, R. Konno, H. Nakano, and M. Kohmoto, Phys. Rev. B **74**, 033413 (2006).

[43] E. Minot, Y. Yaish, V. Sazonova, and P. L. McEuen, Nature (London) **428**, 536 (2004).